

## REVIEW PAPER

10.1002/2016JA022580

## Special Section:

Measurement Techniques in  
Solar and Space Physics:  
Particles

## Key Points:

- MCPs can be made using glass substrates and ALD films
- The resistance, gain, and substrate are independently selectable with ALD MCPs
- ALD MCPs are easily made in curved, nonplanar formats

## Correspondence to:

M. A. Popecki,  
map@incomusa.com

## Citation:

Popecki, M. A., et al. (2016),  
Microchannel plate fabrication using  
glass capillary arrays with Atomic Layer  
Deposition films for resistance and gain,  
*J. Geophys. Res. Space Physics*, 121,  
doi:10.1002/2016JA022580.

Received 21 FEB 2016

Accepted 11 JUL 2016

Accepted article online 23 JUL 2016

## Microchannel plate fabrication using glass capillary arrays with Atomic Layer Deposition films for resistance and gain

M. A. Popecki<sup>1</sup>, B. Adams<sup>1</sup>, C. A. Craven<sup>1</sup>, T. Cremer<sup>1</sup>, M. R. Foley<sup>1</sup>, A. Lyashenko<sup>1,2</sup>,  
M. J. Minot<sup>1</sup>, M. Aviles<sup>1</sup>, J. L. Bond<sup>1</sup>, M. E. Stochaj<sup>1</sup>, W. Worstell<sup>1</sup>, J. W. Elam<sup>3</sup>, A. U. Mane<sup>3</sup>,  
O. H. W. Siegmund<sup>4</sup>, C. Ertley<sup>4</sup>, L. M. Kistler<sup>5</sup>, and M. S. Granoff<sup>5</sup><sup>1</sup>Incom, Inc., Charlton, Massachusetts, USA, <sup>2</sup>Now at Oxford Instruments, Bristol, UK, <sup>3</sup>Argonne National Laboratory, Argonne, Illinois, USA, <sup>4</sup>Space Sciences Laboratory, University of California, Berkeley, California, USA, <sup>5</sup>Space Science Center, University of New Hampshire, Durham, New Hampshire, USA

**Abstract** Microchannel plates (MCPs) have been used for many years in space flight instrumentation as fast, lightweight electron multipliers. A new MCP fabrication method combines a glass substrate composed of hollow glass capillary arrays with thin film coatings to provide the resistive and secondary electron emissive properties. Using this technique, the gain, resistance, and glass properties may be chosen independently. Large-area MCPs are available at moderate cost. Secondary emission films of Al<sub>2</sub>O<sub>3</sub> and MgO provide sustained high gain as charge is extracted from the MCP. Long lifetimes are possible, and a total extracted charge of 7 C/cm<sup>2</sup> has been demonstrated. Background rates are low because the glass substrate has little radioactive potassium 40. Curved MCPs are easily fabricated with this technique to suit instrument symmetries, simplifying secondary electron steering and smoothing azimuthal efficiency.

## 1. Introduction

Microchannel plates (MCPs) are thin, planar structures that contain many small diameter, parallel pores oriented nearly perpendicular to the surface. Incoming ions, electrons, or energetic photons can easily ionize the pore walls. The secondary electrons from the ionization are then drawn down the pore by an electric field. As they strike the walls on the way, they generate additional secondary electrons, until a cascade of about 10,000 are expelled from the bottom end of the pore. The electric field is developed by applying a high voltage from one planar surface of the MCP to the other. Two MCPs may be used in a stack to produce an electron gain of one million electrons or more. Output pulses are fast, rising in 1 nS or less [Milnes and Howorth, 2005].

MCPs are made with glass and have an open area ratio of 60% or more, so they are lightweight. Thicknesses are usually about 0.5 mm to 1.5 mm. Pore diameters can be as small as 2 μm, or as large as 150 μm or more. Their surface area may have arbitrarily formed outlines, so they can conform to the requirements of a wide range of detector configurations.

MCPs are used in applications such as image intensification, night vision devices; photomultipliers for photon and particle detection using scintillators [Matsuura et al., 1985; Akatsu et al., 2004]; UV spectrometers [Priedhorsky et al., 1988; Stock et al., 1993; Sandel et al., 2000; Stern et al., 2007, 2008]; and time of flight (TOF) devices such as terrestrial and space flight mass spectrometers [Gloeckler et al., 1995; Reme et al., 1997; Mason et al., 1998; Galvin et al., 2008]; scanning electron microscopes and residual gas analyzers. Their high gain and lightweight compact structure enable fabrication of low-mass, low-volume particle and photon detectors. They can have large areas and high channel density. Each microchannel acts as a largely independent detector. Therefore, they can provide spatial information, and may be used for imaging, or for extracting information such as particle arrival direction.

The fast signal rise time of the MCP makes possible TOF measurements in the sub-nS regime. These measurements provide the particle speed in mass spectrometry. TOF measurements may also be used to localize radiation sources for gamma rays in positron emission tomography, or light from scintillation in high-energy physics large volume water detectors.

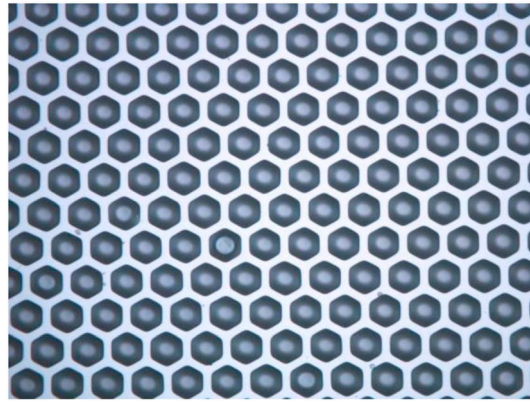


**Figure 1.** A glass capillary array is shown after the drawing, fusing, and wafer slicing operations are complete. Thin films for resistance and SEE will be applied to create an MCP.

## 2. Manufacturing Techniques

Microchannel plates have been made using essentially one technique since the 1960s. Recently, a new approach has been developed, which combines glass capillary array substrates with thin film deposition techniques that provide the necessary resistive and secondary emissive properties of an MCP. There are several advantages to this approach. The glass, the resistive, and the emissive properties may all be chosen independently. The glass can be mechanically robust and may be selected to have a low content of radioactive material for reduction of background activity.

### 2.1. The Traditional MCP Manufacturing Technique

In the traditional process of MCP manufacturing [Wiza, 1979; Price *et al.*, 2002], lead glass tubes are filled with glass rods. The tube and rod assemblies are thermally codrawn, so that the tube collapses around the rod to produce long, slender fibers with a lead glass cladding, and an inner core glass. Fibers are then stacked in parallel and stretched again together. Multiple fiber assemblies are then fused together in parallel. Wafers are cut across the fiber assemblies, where the wafer plane is nearly perpendicular to the axis of the fibers. The core glass is then etched away, leaving an array of pores, each typically about 10–20  $\mu\text{m}$  in diameter. This lead glass capillary array is then heated in the presence of hydrogen, which chemically reduces the surface of the glass, leaving a resistive and emissive surface that is effective for electron amplification.

During use, traditional MCPs typically display an initial reduction in gain, often followed by a slow decline for the remainder of the MCP lifetime. *Then and Pantano* [1990] investigated a possible explanation for the loss of gain. They examined the composition of the surface of the traditional lead glass MCP pore. They found an alkali-rich top surface, about 20–50 nm thick. This layer contained elements such as potassium, cesium, and rubidium. After exposure to 500 eV electrons, with an extracted charge of 0.3 C/cm<sup>2</sup>, the content of potassium and rubidium were reduced, along with a reduction in the gain of the MCP. They suggested that the reduction in alkali element content was the result of electron stimulated desorption and alkali migration within the glass. Citing *Hill* [1976], they suggested that the alkali constituents, including potassium, were essential for secondary electron emission. The potassium in the traditional MCP has a radioactive component. Decays produce secondary electrons in the MCP, which leads to background counts when the MCP is operated [Siegmond *et al.*, 1988].

### 2.2. The Atomic Layer Deposition MCP Manufacturing Approach and Advantages Over Conventional MCPs

The recently developed manufacturing approach for Atomic Layer Deposition (ALD) MCPs starts with capillary tubes drawn from borosilicate glass in a manner similar to conventional MCP manufacturing [Minot *et al.*, 2014]. However, these fibers are hollow, so there is no need to etch away a core. This reduces the cost of manufacturing and practically eliminates any upper limit on the length to diameter ratio ( $l/d$ ) imposed by the etching process. The fused capillary bundles are then sliced in the same manner as in the conventional process, to make flat plates consisting of adjacent pores. These are known as glass capillary arrays (GCAs) and are at the same configuration as the conventional lead glass MCPs after their cores are etched away. A photo of a glass capillary array is shown in Figure 1 after the completion of the glass capillary drawing, the parallel fusing of long capillaries into a block, wafer slicing, and finally polishing. Some water left over from the cleaning process is visible in the channels.

The microchannels adopt a hexagonal shape, which becomes more pronounced in higher open area ratio (OAR), thin wall capillaries. OARs of 74% are easily achievable with this process. A related application of hollow-drawn capillaries is for X-ray concentrators and lenses [Popecki *et al.*, 2015]. These X-ray capillary structures can be as long as 36 cm. They have a composite structure, in which most capillaries have an 83% OAR, and are bundled into multifiber groups, each surrounded with a layer of 60% OAR capillaries for mechanical strength.

The borosilicate glass has a very low concentration of radioactive material such as potassium and therefore has a lower background rate when used for an MCP [Siegmond *et al.*, 1988]. It is also mechanically strong. Borosilicate glass is used for present-day Pyrex glass products. Other glasses may be chosen as appropriate for the application. For example, glass with an enhanced boron 10 component [Tremis *et al.*, 2005] or gadolinium will enhance the MCP sensitivity to thermal neutrons. Thick MCPs with  $l/d$  ratios of  $\sim 500:1$  further improve the probability of neutron detection.

For spaceflight applications, mechanical robustness is needed for the vibration and acoustic environment of launch. Conventional MCPs often need considerable mechanical support to survive vibration. This may limit science performance, for example, by reducing the exposed area of the MCP within the support frame. ALD-coated MCPs exhibit enhanced robustness since the glass substrate may be independently chosen to have the desired mechanical properties. Furthermore, ALD-coated MCPs do not require hydrogen firing and thus avoid embrittlement found in traditional MCPs due to hydrogen diffusing into the glass.

The GCA is converted to an MCP by adding a thin film to establish the desired plate resistance then another to provide a secondary emission layer. The thin film is deposited by the ALD technique. The resistance is chosen according to the application of the MCP. High resistances result in low-power operation, which is useful for spaceflight or portable instruments. Low resistance accommodates high event rates. The emission layers may be  $\text{Al}_2\text{O}_3$ , or  $\text{MgO}$  [Insepov *et al.*, 2010]. The  $\text{Al}_2\text{O}_3$  has good long-term gain stability and durability against exposure to air.  $\text{MgO}$  has an even higher gain [Minot *et al.*, 2014]. Each microchannel has a resistive coating applied by the ALD process. This layer establishes the DC or strip current through the MCP, which recharges the channels after they produce a charge pulse. A secondary electron emission (SEE) layer is applied over the resistive coating as the innermost surface of the pore. The ALD resistive coating is approximately  $0.1 \mu\text{m}$  thick [Mane *et al.*, 2011].

ALD is uniquely suited for applying resistive and emissive layers for the fabrication of MCPs, since other conventional thin film coating techniques, such as vacuum evaporation or sputtering are “line of sight” and cannot effectively coat the inside surfaces of high length to diameter ratio ( $l/d$ ) capillary. The ALD process for each layer is described in Elam *et al.* [2013] and Mane and Elam [2013]. Layers of a metal oxide and a metal were applied to the substrate, which could be a glass capillary array. The metal oxide was aluminum oxide, which has a high resistance, and the metal was Mo, which has a low resistance. The final resistance depended on the relative number of layers of each. MCP thin films use tungsten instead of Mo, but the process is otherwise the same.

The aluminum oxide is applied by exposing the substrate to trimethyl aluminum, followed by an exposure to water. This is repeated several times. Each layer thickness is limited because the number of available chemical bonds is limited. Molybdenum is added by applying a pair of exposures, first to  $\text{S}_2\text{H}_6$ , then to  $\text{MoF}_6$ .

A layer of nichrome is deposited on the top and bottom surfaces of the MCP. The nichrome in both the traditional and alternative approaches forms an electrode that controls the potential on the top and bottom and provides a pathway for restoring charge to be delivered to the MCP pores after a charge pulse. The nichrome layer is approximately  $200 \text{ nm}$  thick. It is applied from a source at a large angle to the microchannel axis so that it only penetrates the channel by about one channel diameter. This creates a conductive surface on the top and bottom of the plate, while leaving the resistive film to control the resistance in the channel.

### 3. Current State of the Art Conventional and ALD MCPs

#### 3.1. Channel Diameter

ALD-coated MCPs have been made with channel diameters as low as  $10 \mu\text{m}$ , using the glass capillary substrate approach. Conventional MCPs have been made with channel diameters as low as  $2 \mu\text{m}$ . A small diameter channel and a thin MCP tend to make the fastest output pulses [Milnes and Howorth, 2005]. Small channel diameters also improve the pulse height distribution and help sustain MCP gain in strong magnetic fields.

#### 3.2. Background Counting

Background counting for a  $20 \text{ cm} \times 20 \text{ cm}$  ALD-coated MCP was measured at less than  $0.078 \text{ counts}/(\text{s cm}^2)$  [Siegmond *et al.*, 2013]. They attributed this to a reduction of radioactive alkali metal content by a factor of 3 to 4 from a conventional MCP formulation. Background rates in similar conventional MCPs have been observed as low as  $0.25 \text{ counts}/(\text{s cm}^2)$  [Siegmond *et al.*, 2013].

Background rates are low for ALD-coated MCPs because the glass substrate may be chosen to have low levels of radioactive materials. This is desirable for low-rate applications such as missions to study interstellar and interplanetary neutrals. Techniques for neutral particle detection tend to have a poor efficiency compared to techniques for charged particle detection. Hence, instruments for neutral particles may observe a particle detection rate that is comparable to the background rates in conventional MCPs.

### 3.3. Secondary Electron Yield

In conventional lead glass MCPs, the secondary electron yield can be as high as an average of 3.5 secondary electrons per primary [Then and Pantano, 1990]. Fijol *et al.* [1991] measured an average of 2.5 for 20–400 keV incident electrons.

In ALD MCPs, secondary electron emission depends in part on the thickness of the secondary emission layer because of the limited electron escape pathlength [Jokela *et al.*, 2012]. It also depends on the incident electron energy and incident angle. Monte Carlo calculations of secondary electron emission from  $\text{Al}_2\text{O}_3$  have been performed as a function of incident electron energy and angle [Insepov *et al.*, 2010]. These calculations indicate that a secondary electron yield of  $\sim 6$  is possible. The secondary electron escape length for this calculation was 60 Å. Measured values for  $\text{Al}_2\text{O}_3$  secondary electron emission have been observed as high as 2.8, and as high as 7 for MgO secondary emission electron emission [Jokela *et al.*, 2012]. The electron beam for this work was perpendicular to the surface.

### 3.4. Gain and Extracted Charge: Lifetime and Spatial Uniformity

Extracted charge is one of the most important features of microchannel plates. In planetary or solar heliospheric missions, the long flight duration in interplanetary space demands significant extracted charge. Although a long duration might be nominally 5 years or more, the MCP lifetime depends on the intensity of the radiation to be monitored. For example, a solar wind mass spectrometer will encounter a large dynamic range of intensity between H and Fe. Design trade-offs must be made to manage this range, which may result in a relatively high charge extraction rate from H to maintain counting statistics for Fe. The instrument will also encounter penetrating radiation from coronal mass ejections (CMEs), particularly if the mission approaches the Sun.

Moreover, the design of the instrument may concentrate the incoming ions in a localized area of a microchannel plate, thereby increasing charge extraction in this region. Kistler *et al.* [2013] discussed in-flight calibration for the Cluster/CODIF mass spectrometer during its mission in the Earth's magnetosphere. The gain of the MCPs decreased during the mission, causing a reduction of ion detection efficiency by a factor of 50 over a 12 year period. This instrument design used large-area MCPs and a single high-voltage supply to simplify the mechanical structure. However, spatially concentrated extracted charge and loss of gain locally reduced detection efficiency and caused operational limitations on high voltage. Gain may be temporarily restored in these areas by increasing the MCP voltage; however, the rest of the MCP will operate at a much higher gain. The high gain areas will produce large pulses that can create crosstalk in timing electronics and high output currents that may cause a shutdown of the high-voltage supply.

Griffiths *et al.* [1998] described the reduction of gain in the SOHO/Solar Ultraviolet Measurements of Emitted Radiation UV spectrometer. This spacecraft observes the Sun at the L1 position, which is at the gravity balance point between the Earth and the Sun, about 1.5 million km away from the Earth. The instrument is exposed to solar UV and occasionally CMEs. It had two sets of MCPs. The gain of the first set decreased to less than 10% of its original value in less than 1 year. The result was that some events fell below the electronics threshold and were not detected. This set of MCPs was used from December 1995 to September 1996. The second set of MCPs experienced a similar loss of gain in about 1 year.

In solar wind mass spectrometers, a total charge extraction on the order of  $10\text{ C/cm}^2$  could be needed for a multiyear mission close to the Sun or to a planet with significant populations of energetic particles trapped in radiation belts. Extracted charge capability of  $50\text{--}100\text{ C/cm}^2$  would provide significant margin for these long-term missions. Ongoing life testing of ALD MCPs will determine if they can make significant progress toward this goal. Initial results are promising.

As stated above, conventional MCPs exhibit a charge extraction behavior in which the gain rapidly decreases over the first  $0.3\text{ C/cm}^2$  extracted from the plates, after which the gain decreases at a lower rate for the

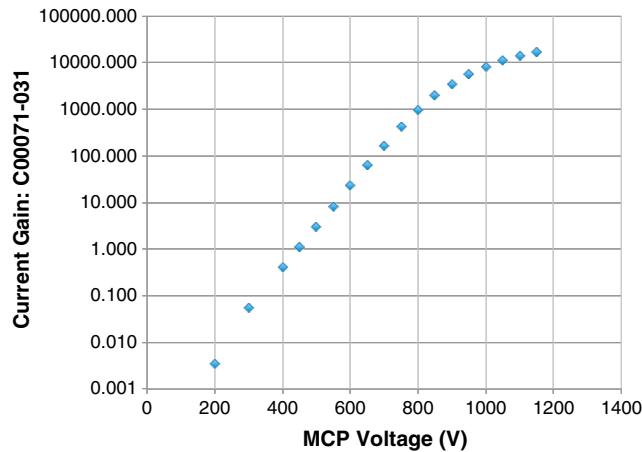


**Figure 2.** The gain is shown for an 8 inch square, single ALD MCP, with an Al<sub>2</sub>O<sub>3</sub> SEE layer and 20 micron pores.

above, the gain decreases with the first 0.3 C/cm<sup>2</sup> of extracted charge, then continues to decrease, but at a slower rate. However, ALD MCPs with MgO as the secondary emission layer feature an initial increase in gain, after which the gain remains high for an extracted charge of several C/cm<sup>2</sup>. Siegmund et al. [2013] presented the gain for a pair of MCPs with an ALD MgO secondary emission layer. The gain rose after a bakeout and then stabilized. This initial gain was attributed to compounds formed between the MgO and water during exposure to air. The bakeout, or alternatively exposure to UV during operation, appears to remove these compounds. They also performed a life test of an MgO MCP pair. It shows relatively stable gain out to a charge extraction of 7 C/cm<sup>2</sup>.

The gain for a single ALD-coated MCP is shown as a function of voltage in Figure 2, with an Al<sub>2</sub>O<sub>3</sub> SEE film. This measurement was performed at Incom. A gain of 10,000 was reached at an applied voltage of 1000V. The measurement was made by applying a small input current on the order of a few nanoamperes to the MCP, then increasing the voltage across the MCP, and measuring the output current to an anode. The ratio of the output current to the constant input current was reported as the gain. The input current to the MCP under test was produced by another MCP that was mounted in a parallel, face-to-face arrangement, with a small, ~1 mm gap in between.

A conventional lead glass MCP may be overcoated with an ALD SEE layer such as Al<sub>2</sub>O<sub>3</sub> or MgO. However, the flexibility of independently choosing the glass substrate for advantages in additives, low background, or

lifetime of the plate [Siegmund et al., 2013]. The gain may be restored temporarily by raising the MCP voltage, until the MCP reaches the end of its useful life. However, there are limits to the maximum applied voltage for safe operation of the MCP, and the power budget for the instrument must accommodate the higher end-of-life power. This can be problematic for power-constrained, long-duration missions.

Total extracted charge from a conventional lead glass MCP may be on the order of 10 C/cm<sup>2</sup> [see, e.g., Griffiths et al., 1998]. As described

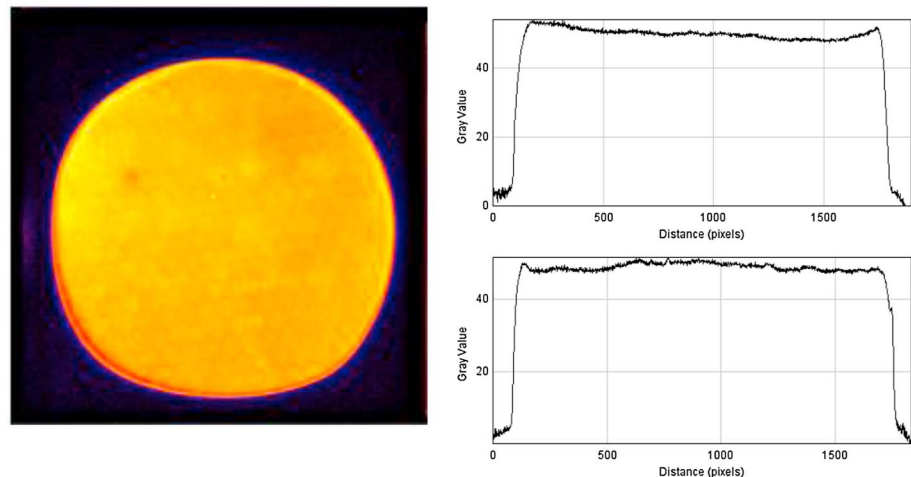


**Figure 3.** (left) A gain map of a 33 mm diameter MgO ALD MCP chevron pair is shown. (right) Horizontal and vertical profiles of the image display good spatial gain uniformity.

mechanical strength, is not achieved. The technique of overcoating a conventional MCP was used by *Conneely et al.* [2013] to investigate the role of ion feedback as a cause of photocathode damage in an MCP photomultiplier tube.

Gain spatial uniformity has also been demonstrated with ALD MCPs. A spatial gain map of an MgO ALD MCP is shown in Figure 3 (left). Horizontal and vertical sectional profiles are shown in Figure 3 (right column). The gain variation is approximately 10% across the surface. The gain is somewhat higher at the edges in this case, but the distribution may be different for other ALD MCPs. The uniformity depends in part on the uniformity of the ALD constituent gas flow in the reactor. The flow in turn can be influenced by the fixturing that holds the glass capillary arrays. The hexagonal pattern in the image comes from the assembly process of glass capillary bundles.

#### 4. Application: Extension of the Lifetime of MCP Photomultiplier Tubes Using ALD MCPs

MCPs may be used in photomultiplier tubes instead of the traditional dynode chain. The benefit is a more compact envelope and faster output pulses—subnanoseconds instead of microseconds. This type of device is used in UV spectrometers [*Stern et al.*, 2007]. However, the lifetime of these devices is typically limited by the photocathode. This is because the electron cascade can sputter ions from the MCP pores in a process known as ion feedback. The ions are driven out of the entry side of the MCP by the same electric field that causes electron multiplication and then they collide with the photocathode. The impact damages the photocathode and shortens its usable life. One approach to limit this damage is to apply a thin window film on the top surface of the MCP closest to the photocathode [*Kishimoto et al.*, 2006]. The film must be thick enough to serve as a barrier to the ions, yet thin enough to allow input electrons with energies of  $\sim 100$ – $200$  eV from the photocathode to enter the pores.

Recent use of ALD coatings has extended the lifetime of an MCP-PMT to  $6\text{ C/cm}^2$  [*Lehmann et al.*, 2014]. *Lehmann et al.* [2014] proposed that the ALD coating tends to confine the ions in the channel wall, reducing impact damage to the photocathode. The lifetime of a conventional MCP-PMT was compared to the lifetime of an ALD MCP-PMT by *Conneely et al.* [2013]. The total extracted charge for the conventional unit was only  $0.3\text{ C/cm}^2$ , while it was at least  $5\text{ C/cm}^2$  for the ALD unit.

##### 4.1. Pulse Rise Time in an ALD MCP

Fast pulse rise times in MCPs improve timing measurements. Fast fall times minimize pulse pileup in high-rate conditions. Rise times should generally become smaller for smaller diameter pore MCPs with the same  $l/d$  ratio, because the secondary electrons have a shorter path to the end of the pores [*Matsuura et al.*, 1985]. Rise times may also be affected by the electric field between output side MCP and the anode. As the electric field becomes stronger, the rise times tend to become shorter, but with diminishing returns near  $\sim 100$ – $600$  V/mm [*Martindale et al.*, 2007; *Milnes and Howorth*, 2005].

The temporal behavior of a pair of 10 micron pore, 33 mm diameter, ALD MgO-coated microchannel plates was evaluated at a laser facility at the Argonne National Laboratory. The facility is described in *Wetstein* [2012] and *Adams et al.* [2013]. A brief laser pulse was applied through a window to a detector assembly in a vacuum chamber (Figure 4, left). The detector consisted of a stack assembly of an aluminum photocathode, a pair of 10  $\mu\text{m}$  MCPs and an anode. The time profiles of the MCP pulses were recorded.

The laser was a Ti:Sapphire laser with pulse widths of less than 100 femtoseconds. For timing purposes, the laser pulse was detected by directing it through a beam splitter. One branch of the beam splitter output was detected by a photodiode. The photodiode had a fast output pulse with a rise time of about 100 pS. This was used to trigger an oscilloscope measurement of the MCP pulse, downstream from the laser. Applying an electric field of 71 V/mm between the exit MCP and anode, the average rise time of the MCP pulses was 647 pS. A sample laser pulse and MCP pulse waveform are shown in Figure 4 (right). In this case, the electric field was 143 V/mm, and the rise time of this pulse was 619 pS, and the fall time was 492 pS.

#### 5. MCP Resistance Versus Temperature

MCP resistance decreases at increasing temperatures [*Roth and Fraser*, 2000]. The relationship is as follows:

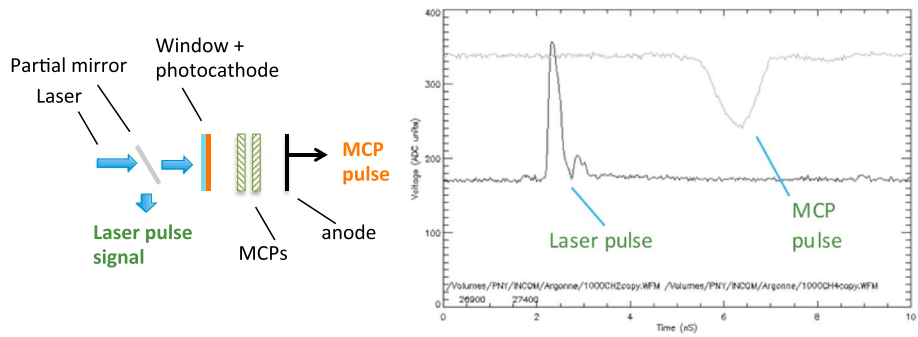


Figure 4. Pulse timing is shown for an ALD MCP. The pulse rise time is ~0.65 nS.

$$R(T) = R_0 \exp(-\alpha(T - T_0))$$

where  $R_0$  is the resistance at an initial temperature  $T_0$ . The temperature coefficient  $\alpha$  is typically 0.01 to 0.02 for conventional MCPs [Roth and Fraser, 2000; Siegmund, 1989; Pearson et al., 1987; Fraser et al., 1988; Slater and Timothy, 1993], while it is somewhat higher for MCPs with an ALD resistive coating. A higher value of  $\alpha$  corresponds to a larger variation of resistance with temperature. A measurement of resistance as a function of temperature for an ALD-coated silicon sample was performed by Mane and Elam [2013], using molybdenum as the metal. Molybdenum is one of many metals that have been shown to be effective for ALD MCPs. A comparison of their results to conventional lead glass MCP behavior is made in Figure 5. The resistance of the ALD MCP sample is plotted as a function of temperature. Also plotted is the expected variation of resistance with temperature for conventional MCPs, using the thermal coefficients of 0.01 and 0.02. The ALD-coated sample has a steeper change of resistance with temperature and a temperature coefficient  $\alpha$  of 0.03.

Resistance stability as a function of temperature is important for MCPs that will be changing thermal environments. A typical operational temperature range for a spaceflight instrument is  $-25\text{C}$  to  $+40\text{C}$ . Survival temperatures can be  $10^\circ$  outside this range. Although instruments are thermally designed to operate at a target temperature, for example,  $25^\circ\text{C} \pm 5^\circ\text{C}$ , they have to be able to tolerate deviations that may result from attitude or orbital changes. Earth-orbiting missions with highly elliptical, nearly equatorial orbits may spend enough time in the Earth’s shadow for the instrument temperature to change. Missions to distant regions start near the Earth, where instrument commissioning is done. However, the instruments are designed to reach their target temperature at the destination environments, for example, hot locations near the Sun or cold locations at the outer planets. Temperatures may reach either end of the range during this transition period. MCPs tend to draw the most power in an instrument, even in the optimal environment. At a constant MCP voltage, power will go inversely with resistance. A 10% resistance and therefore power variation over the operational temperature range is desirable. In hotter locations during the phasing orbits, the MCP high-voltage supply must be sized to provide sufficient power to handle the lower resistance MCP. This may be again difficult for power-constrained missions. If an MCP is intended to operate in a hot environment, it may be fabricated with a high resistance at room temperature. However, high resistance limits the event rate of the MCP, because it reduces the recharge current needed to refresh the MCP channels after a pulse. This may be problematic during ground testing and early orbit commissioning.

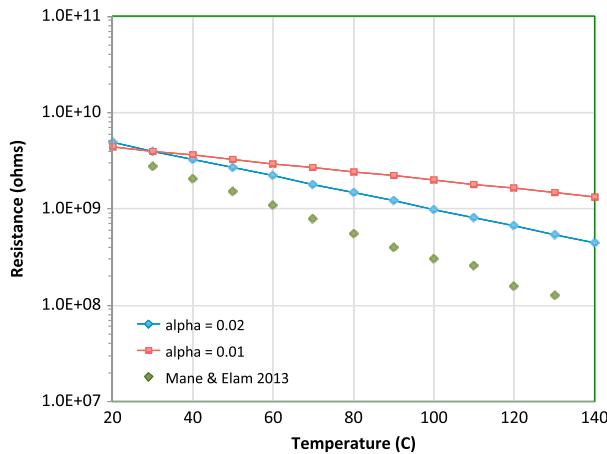


Figure 5. The relation of MCP resistance to temperature is shown for conventional MCPs [Roth and Fraser, 2000] and an ALD-coated sample [Mane and Elam, 2013].

ALD MCPs presently have a steep relationship between temperature and resistance, because of the nature of the resistive film that is typically used. However, ALD-coated MCPs have the potential to be made with a flatter resistance response to temperature by changing the composition of the film. The metals and metal oxides in the ALD coatings have the opposite sign temperature coefficient, so the appropriate mix may produce a flat response.

A flat thermal response will also prevent MCP thermal runaway. This is a condition in which an MCP is heated during operation, which causes a decrease in resistance, which in turn causes further heating. Eventually, either a high-voltage current limit will be reached, or the MCP will possibly be damaged. The electrical heat input to the MCP is applied at the edges where the contacts are made. The heat is dissipated from the exposed surface area by radiation. Stable operation requires a balance between the input of electrical heat plus the radiated heat from the environment and the radiated heat output from the MCP surface. In hot environments, or in MCPs with either a low initial resistance or small surface area, the net heating budget can increase the temperature of the MCP and begin the runaway process. Thermal runaway cannot be eliminated from a conventional MCP, but it could be minimized or eliminated for ALD MCPs by altering the resistive film composition.

The spatial temperature distribution from the electrical contact at the edge of MCP outward to the exposed area of the MCP was modeled by *Matsuura et al.* [1984] for various MCP resistances. A 10 M $\Omega$  MCP with 1000 V applied was calculated to be  $\sim 20$  C higher in the exposed area than at the edge clamp. The heating process and thermal runaway effect was later modeled by *Tremsin et al.* [2004]. *Tremsin et al.* [1996] discussed low resistance MCPs that were used under high event rates but cooled to avoid thermal runaway.

## 6. Curved MCPs

Curved MCPs have been used in UV spectrometers to match the detector to the geometry of the overall instrument [*Stern et al.*, 2007]. In particle instruments such as mass spectrometers, curved MCPs may be used to improve time of flight resolution by matching natural geometrical symmetries within the instrument housing. For example, an instrument with a top hat electrostatic analyzer and a 360° field of view may use cylindrically curved MCPs to efficiently detect secondary electrons used to measure the time of flight of incoming ions. They may also be used to optimize the use of interior volume and therefore reduce instrument mass in a compact mass spectrometer [e.g., *Reme et al.*, 1997; *Galvin et al.*, 2008].

Ion mass spectrometers often use secondary electrons created by ion passage through a carbon foil window or by a collision with a solid state detector (SSD) to measure time of flight. The detection of secondary electrons can be compromised by two factors: variations in flight time from source to MCP and variations in the angle of incidence to the MCPs. Variations in flight time can occur because of nonuniformities in steering electric fields within the instrument, particularly when flight paths for secondary electrons are long. Variations can also be caused by the differences in initial trajectories and speeds of secondary electrons as they leave the carbon foil. Additionally, secondary electrons may hit other structures within the instrument, including those that hold segmented MCPs, and go on to strike the target MCP, therefore creating an anomalous timing signal.

Long, curved MCPs may be used in mass spectrometers to simplify the detector geometry and minimize the structures needed to hold instrument components together. This in turn reduces the electrostatic disruption of secondary electron flight paths. Simplification can simultaneously improve the use of the interior instrument volume. Volume otherwise needed to adapt nonplanar instrument geometries to planar MCPs, such as with cylindrically symmetric instruments, may be used instead to house support devices such as high-voltage supplies or processing electronics.

The angle between the incident secondary electron and the MCP microchannel affects the probability for electron detection. *Gao et al.* [1984] measured MCP detection efficiencies for ions and found a sharp rise in efficiency for incident angles of 2 to 7°. There was a peak near 10°, and a slowly decreasing efficiency for larger incident angles. *Galanti et al.* [1971] found a peak in detection efficiency at about 15° for 1 keV electrons. Planar MCPs have a fixed pore orientation, which must be aligned in one direction. Incident secondary electrons from all other directions will have different incoming angles with respect to the pores, and therefore different efficiencies for detection. This adds complexity to the instrument response function. Curved MCPs eliminate this problem. They have a fixed pore orientation with respect to the local normal to the surface. Incoming secondary electrons in a curved, symmetrical geometry may therefore have the same incident angle to the pores, and the same detection efficiency across the field of view.

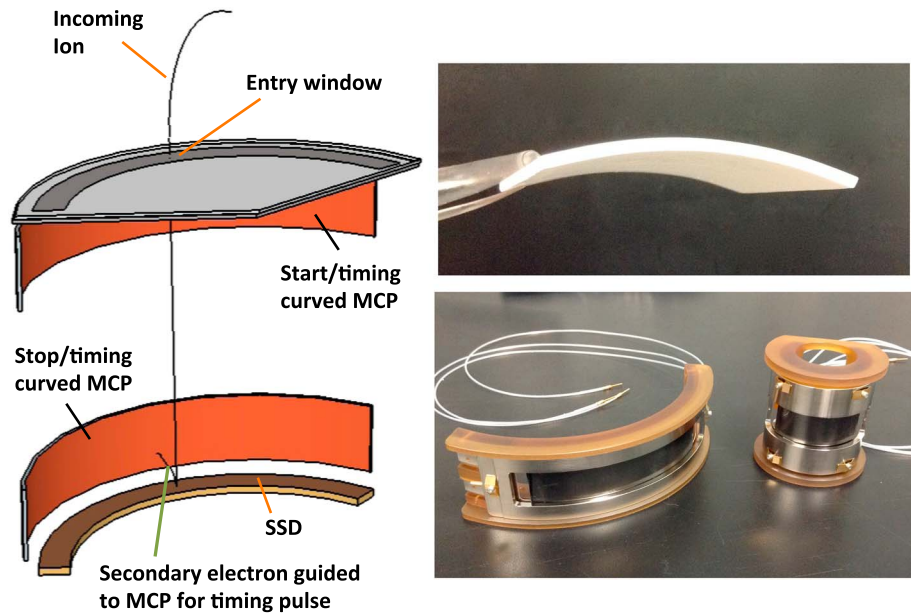


**Figure 6.** (left) A sample application of curved MCPs is shown for a cylindrically symmetrical mass spectrometer. (top right) A curved glass capillary array is shown prior to coating with thin films for resistance and SEE. (bottom right) Two sets of cylindrically curved ALD MCPs have been made, with radii of curvature of 75 and 20 mm.

An example of how curved MCPs could be mounted in a cylindrically symmetric instrument with a window and a solid state detector for time of flight and energy measurements is shown in Figure 6 (left). The MCPs can have a curvature to match the instrument housing. The MCPs can be placed close to the entry window and to the SSD Stop plane. Secondary electrons from ion passage through a window or from impact with an SSD will have a short flight path to a nearby MCP. Short, simple flight paths will improve time of flight resolution, azimuthal resolution, and angle of incidence. They will also be far less sensitive to the disruptive effects of structures. The adjacent arrangement of MCPs in Figure 6 prevents ion feedback from one MCP, as discussed in section 3.3, from creating an anomalous timing signal in an opposing MCP. The perpendicular arrangement of the SSD and MCP also eliminates ion feedback from the SSD to the MCP.

An approximation to curved MCPs may be obtained by tiling small planar sections. However, each must have its own clamp and be supported in framework that forms an arc. These structures must be carefully connected to survive launch vibration. The clamping of each MCP creates dead zones between plates, where measurements cannot be made. Clamping fixtures also electrostatically disrupt the flight of secondary electrons. These significant complications discourage this approach.

An estimate for the loss of detection efficiency from tiling may be made for the instrument example shown in Figure 6 (left). A 90°, 75 mm radius curved MCP may be replaced by three flat MCPs, arranged end to end. A small loss of efficiency will occur because of the variation of the incident electron angle. If the microchannels are oriented at 13° below horizontal to maximize detection efficiency and minimize angular variation, then the incident electron angle will be 13° at the center of a flat MCP section, and 20° at the end. This will result in a loss of detection efficiency of a few percent [Galanti *et al.*, 1971] at the end.

A larger loss of detection efficiency will occur because of clamping hardware. If each MCP has a clamping zone extending 3 mm in from the edge, and if the adjoining clamps only create 3 mm of dead zone between the MCP segments, the loss of detection area will be 19%. These clamps will not only reduce the detection area but will also serve as scattering centers for incident electrons.

### 7. Fabrication of Curved ALD MCPs

Curved microchannel plate chevron pairs have been fabricated in two sizes at Incom and tested for azimuthal gain uniformity (Figure 6, right column). The larger size had a 75 mm radius of curvature and was 25 mm along the axis of curvature. It had a mating MCP with a 76.5 mm radius of curvature to accommodate the thickness of

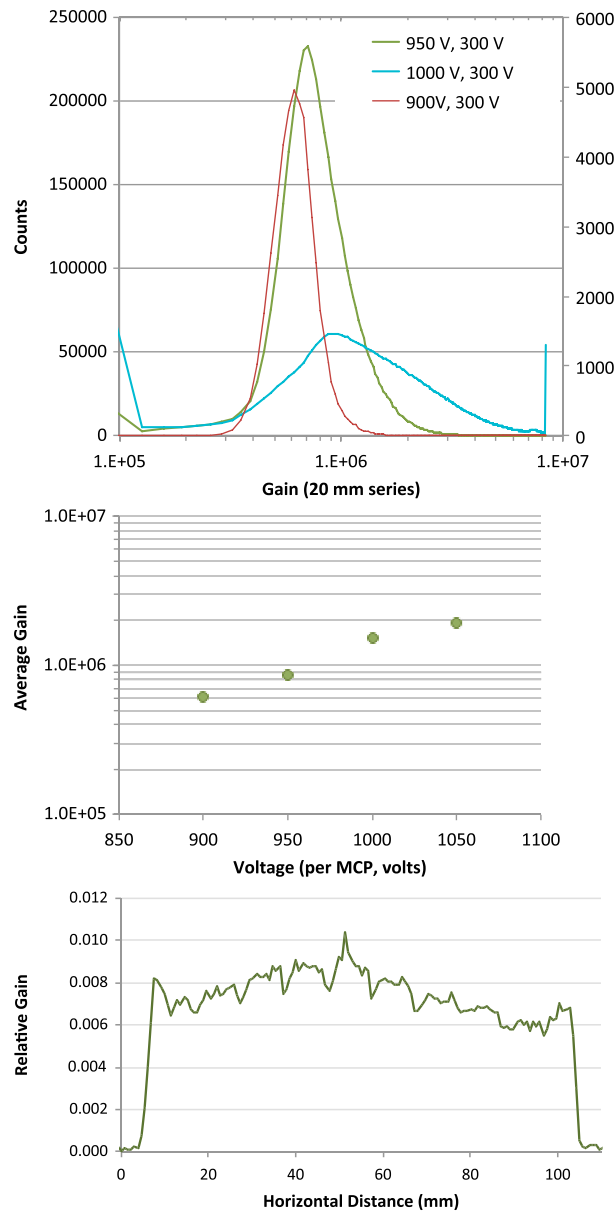


**Figure 7.** (top) Pulse height distributions are shown for the 20 mm radius MCPs. (middle) Gain is shown versus MCP voltage for the 75 mm MCPs. (bottom) Relative gain versus azimuth is shown for the 75 mm MCPs across a  $\sim 70^\circ$  azimuth.

The MCPs were illuminated with a mercury UV lamp from the center of curvature side. The output electrons from the curved MCPs were collected onto the flat anode. The pulse height distributions were generally well formed and easily detected above a fixed threshold (Figure 7, top). Gain for the 75 mm pair is shown versus voltage in Figure 7 (middle). The gain for both types of MCPs was modest, reaching about  $2.5E6$  for the 20 mm series and  $1.5E6$  for the 75 mm series at 1000 V per MCP.

Gain for the 75 mm pair is shown versus lateral distance on the anode in Figure 7 (bottom). This distribution is the projection of a curved MCP surface onto the flat anode surface. The azimuthal gain uniformity for the 75 mm MCPs was  $\pm 20\%$  across the angular span of  $70^\circ$ . The periodic dips in the relative gain panel of Figure 7 were created artificially by structural features in the anode. Additional tests will be performed in which the MCPs are rotated past the anode, to measure gain in segments with a uniform distance between the MCP and anode. Spatial gain variations not associated with projection effects may be created by

the inner MCP. This chevron pair spanned  $\sim 70^\circ$  of arc. MCP chevron pairs having this radius would be useful in spaceflight mass spectrometers that are currently in use.

The smaller size had a chevron pair with 20 and 21.5 mm radii of curvature and is also 25 mm wide. This sample covers  $\sim 160^\circ$  of arc and serves as a likely lower limit of curvature needed for instrumental use.

The glass substrates for both series of MCPs were first bent over forming mandrels and then coated with a resistive film composed of tungsten and  $Al_2O_3$ . The secondary emissive layer was pure  $Al_2O_3$ .

The first production pairs of each size were tested for gain and azimuthal gain uniformity. The curved MCPs were placed near a flat imaging delay line anode, so that the center of the outer curve was approximately 1 cm away from the anode. A single high voltage was applied to the entry side of the MCP pair at the inner curve (see the test fixture in Figure 6, bottom right). The MCPs were separated by a thin nickel contact, with no potential difference between them. The exit face of the exit MCP at the outer curve was held at 200 V below ground. This potential difference was intended to accelerate output electrons to the anode and minimize variations in their flight paths. The electric field between the MCP and anode was strongest in the center of the MCP, and weakest at the ends because of the larger distance between the MCP and the anode there.

nonuniformities in the ALD coating approach for the curved surfaces. Ensuring azimuthal coating uniformity is the subject of ongoing development.

## 8. Conclusions and Outlook

Microchannel plates have enabled measurements such as UV spectrometry or time of flight mass spectrometry, in the resource-limited space instrumentation environment. These applications require electron multiplication with fast timing pulses, spatial resolution, and low mass. Conventional MCPs, available since the 1960s, have served well in spaceflight instrumentation. However, ALD MCPs combining glass capillary array substrates with ALD films offer valuable improvements. Sustained high gain over the lifetime of the MCP will minimize localized gain depression in applications where small areas of a large MCP are preferentially illuminated. Glass substrates may be chosen independently of resistance and secondary electron emission material, enabling MCP designs that better suit the application. Glass substrates may be selected with low radioactive potassium content for low background counting. Glass may also be chosen for mechanical strength to withstand high vibration load launches to distant locations. Curved MCPs are possible, because the glass substrate may be formed to nearly any shape, then coated as needed to introduce the functionality of an MCP. Curved MCPs made in this manner will facilitate instrumentation that would not be practical because of intricate support structures and the impact of launch vibrations. Indeed, a nonplanar MCP such as a cylindrical section may acquire additional stiffness because of its shape. The temperature-dependent resistance of MCPs may also be addressed with the substrate/ALD approach by changing the composition of the resistive film. Although ALD MCPs presently have a steeper relationship between temperature and resistance than conventional MCPs, the ALD technique offers the prospect of flattening the relationship more than in conventional MCPs. Efforts toward this goal are presently underway. These advances in microchannel plate technology will provide a substantial benefit to resource-constrained missions, either in Earth orbit, or elsewhere in the heliosphere.

### Acknowledgments

The work on curved MCPs was supported by the NASA SBIR Phase I contract NNX15CG22P. We note that there are no data sharing issues since all of the numerical information is provided in the figures. The authors would like to thank the anonymous reviewers for their insightful comments and suggestions that have improved this paper.

### References

- Adams, B., M. Chollet, A. Elagin, E. Oberla, A. Vostrikov, M. Wetstein, R. Obaid, and P. Webster (2013), A test facility for large area microchannel plate detector assemblies using a pulsed sub-picosecond laser, *Rev. Sci. Instrum.*, *84*, 061301, doi:10.1063/1.4810018.
- Akatsu, M., et al. (2004), MCP-PMT timing property for single photons, *Nucl. Inst. Methods Phys. Res. A*, *528*, 763–775, doi:10.1016/j.nima.2004.04.207.
- Conneely, T. M., J. S. Milnes, and J. Howarth (2013), Extended lifetime MCP-PMTs: Characterisation and lifetime measurements of ALD coated microchannel plates, in a sealed photomultiplier tube, *Nucl. Inst. Methods Phys. Res. A*, *732*, 388–391, doi:10.1016/j.nima.2013.07.023.
- Elam, J., et al. (2013), Synthesis, characterization, and application of tunable resistance coatings prepared by Atomic Layer Deposition, *ECS Trans.*, *58*(10), 249–261, doi:10.1149/05810.0249ecst.
- Fijol, J. J., A. M. Then, G. W. Tasker, and R. J. Soave (1991), Secondary electron yield of SiO<sub>2</sub> and SiAlN<sub>4</sub> thin films for continuous dynode electron multipliers, *Appl. Surf. Sci.*, *48/49*, 464–471, doi:10.1016/0169-4332(91)90376-U.
- Fraser, G. W., J. F. Pearson, J. E. Lees, and W. B. Feller (1988), Advances in microchannel plate detectors, *Proc. SPIE*, *982*, 98–107.
- Galanti, M., R. Gott, and J. F. Renaud (1971), A high resolution, high sensitivity channel plate image intensifier for use in particle spectrographs, *Rev. Sci. Instr.*, *42*, 1818–1822, doi:10.1063/1.1685013.
- Galvin, A. B., et al. (2008), The Plasma and Suprathermal Ion Composition (PLASTIC) Investigation on the STEREO Observatories, *Space Sci. Rev.*, *136*(1–4), 437–486, doi:10.1007/s11214-007-9296-x.
- Gao, R. S., P. S. Gibner, J. H. Newman, K. A. Smith, and R. F. Stebbings (1984), Absolute and angular efficiencies of a microchannel plate position-sensitive detector, *Rev. Sci. Instr.*, *55*, 1756–1759, doi:10.1063/1.1137671.
- Gloeckler, G., et al. (1995), The solar wind and suprathermal ion composition investigation on the WIND spacecraft, *Space Sci. Rev.*, *71*, 79–124, doi:10.1007/BF00751327.
- Griffiths, N. W., S. Airieau, and O. H. Siegmund (1998), In-flight performance of the SUMER microchannel plate detectors, *Pro. SPIE*, *3445*, 566–577.
- Hill, G. E. (1976), Secondary electron emission and compositional studies on channel plate glass surfaces, *Adv. Electron. Electron Phys.*, *40*(Part A), 153–165.
- Insepov, A., V. Ivanov, and H. Frisch (2010), Comparison of candidate secondary electron emission materials, *Nucl. Instr. Methods Phys. Res. B*, *268*, 3315–3320, doi:10.1016/j.nimb.2010.08.002.
- Jokela, S. J., I. V. Veryovkin, A. V. Zinovev, J. W. Elam, A. U. Mane, Q. Peng, Z. Insepov, and Large Area Picosecond Photodetector Collaboration (2012), Secondary electron yield of emissive materials for large-area micro-channel plate detectors: Surface composition and film thickness dependencies, *Phys. Procedia*, *37*, 740–747, doi:10.1016/j.phpro.2012.03.718.
- Kishimoto, N., M. Nagamine, K. Inami, Y. Enari, and T. Ohshima (2006), Lifetime of MCP PMT, *Nucl. Inst. Methods Phys. Res. A*, *564*, 204–211, doi:10.1016/j.nima.2006.04.089.
- Kistler, L. M., C. G. Mouikis, and K. J. Genestreti (2013), In-flight calibration of the Cluster/CODIF sensor, *Geosci. Instrum. Method. Data Syst.*, *2*, 225–235, doi:10.5194/gi-2-225-2013.
- Lehmann, A., et al. (2014), Improved lifetime of microchannel-plate PMTs', *Nucl. Instr. Methods Phys. Res. A*, *766*, 138–144, doi:10.1016/j.nima.2014.04.005.
- Mane, A., and J. Elam (2013), Nanostructured composite thin films with tailored resistivity by atomic layer deposition, *Proc. SPIE*, *8818*, 88180M, doi:10.1117/12.2024482.

- Mane, A., Q. Peng, M. J. Wetstein, R. G. Wagner, H. J. Frisch, O. H. W. Siegmund, J. M. Michael, B. W. Adams, M. C. Chollet, and J. W. Elam (2011), A novel atomic layer deposition method to fabricate economical and robust large area microchannel plates, *Proc. SPIE*, 8031, 80312H, doi:10.1117/12.882885.
- Martindale, A., J. S. Lapington, and G. W. Fraser (2007), Photon counting with small pore microchannel plates, *Nucl. Instr. Methods Phys. Res. A*, 573, 111–114, doi:10.1016/j.nima.2006.11.005.
- Mason, G. M., et al. (1998), The Ultra-Low-Energy Isotope Spectrometer (ULEIS) for the ACE spacecraft, *Space Sci. Rev.*, 86, 409–448, doi:10.1023/A:1005079930780.
- Matsuura, S., S. Umabayashi, C. Okuyama, and K. Oba (1984), Current status of the micro channel plate, *IEEE Trans. Nucl. Sci.*, 31(1), 399–403, doi:10.1109/TNS.1984.4333286.
- Matsuura, S., S. Umabayashi, C. Okuyama, and K. Oba (1985), Characteristics of the newly developed MCP and its assembly, *IEEE Trans. Nucl. Sci.*, 32, 350–354, doi:10.1109/TNS.1985.4336854.
- Milnes, J., and J. Howorth (2005), Picosecond time response characteristics of microchannel plate PMT detectors, *Proc. SPIE*, 5580, 730–740, doi:10.1117/12.568180.
- Minot, M. J., et al. (2014), Pilot production & commercialization of LAPPD™, *Nucl. Instr. Methods Phys. Res. A*, 787, 78–84, doi:10.1016/j.nima.2014.11.025.
- Pearson, J. F., et al. (1987), Variation of microchannel plate resistance with temperature and applied voltage, *Nucl. Instr. Methods Phys. Res. A*, 258(2), 270–274, doi:10.1016/0168-9002(87)90069-6.
- Popecki, M. A., et al. (2015), Development of polycapillary X-ray optics for synchrotron spectroscopy, *Proc. SPIE*, 9588, doi:10.1117/12.2188687.
- Price, G. J., A. N. Brunton, M. W. Beijersbergen, G. W. Fraser, M. Bavdaz, J.-P. Boutot, R. Fairbend, S.-O. Flyckt, A. Peacock, and E. Tomaselli (2002), X-ray focusing with Wolter microchannel plate optics, *Nucl. Instr. Methods Phys. Res. A*, 490, 276–289, doi:10.1016/S0168-9002(02)01059-8.
- Priedhorsky, W. C., J. J. Bloch, B. W. Smith, K. Strobel, and M. Ulibarri (1988), ALEXIS: An ultrasoft X-ray monitor experiment using miniature satellite technology, *Proc. SPIE*, 982, 188–207.
- Reme, H., et al. (1997), The Cluster Ion Spectrometry (CIS) experiment, *Space Sci. Rev.*, 79, 303–350, doi:10.1023/A:1004929816409.
- Roth, P., and G. W. Fraser (2000), Microchannel plate resistance at cryogenic temperatures, *Nucl. Instr. Methods Phys. Res. A*, 439, 134–137, doi:10.1016/S0168-9002(99)00792-5.
- Sandel, B. R., et al. (2000), The extreme ultraviolet imager investigation for the IMAGE mission, *Space Sci. Rev.*, 91, 197–242, doi:10.1023/A:1005263510820.
- Siegmund, O. H. W. (1989), Preconditioning of microchannel plate stacks, *Proc. SPIE*, 1072, 111–118.
- Siegmund, O. H. W., J. Vallergera, and B. Wargelin (1988), Background events in microchannel plates, *IEEE Trans. Nucl. Sci.*, 35, 524–528, doi:10.1109/23.12778.
- Siegmund, O. H. W., et al. (2013), Performance characteristics of atomic layer functionalized microchannel plates, *Proc. SPIE*, 8859, 88590Y, doi:10.1117/12.2024919.
- Slater, D. C., and J. G. Timothy (1993), Microchannel plate modal gain variations with temperature, *Rev. Sci. Instr.*, 64, 430–435, doi:10.1063/1.1144212.
- Stern, S. A., et al. (2007), ALICE: The Rosetta ultraviolet imaging spectrograph, *Space Sci. Rev.*, 128, 507–527, doi:10.1007/s11214-006-9035-8.
- Stern, S. A., et al. (2008), ALICE: the ultraviolet imaging spectrograph aboard the New-Horizons Pluto-Kuiper Belt mission, *Space Sci. Rev.*, 140, 155–187, doi:10.1007/s11214-008-9407-3.
- Stock, J., O. H. W. Siegmund, M. Hurwitz, R. Raffanti, C. Stuart Bowyer, and M. L. Lampton (1993), The Berkeley EUV spectrometer microchannel plate detectors for ORFEUS, *Proc. SPIE*, 2006, 128–138.
- Then, A. M., and C. G. Pantano (1990), Formation and behavior of surface layers on electron emission glasses, *J. Non Cryst. Solids*, 120, 178–187, doi:10.1016/0022-3093(90)90202-W.
- Tremsin, A. S., J. F. Pearson, G. W. Fraser, W. B. Feller, and P. White (1996), Microchannel plate operation at high count rates: New results, *Nucl. Instr. Methods Phys. Res. A*, 379, 139–151, doi:10.1016/0168-9002(96)00482-2.
- Tremsin, A. S., J. V. Vallergera, O. H. W. Siegmund, C. P. Beetz, and R. W. Boerstler (2004), Thermal dependence of electrical characteristics of micromachined silica microchannel plates, *Rev. Sci. Instr.*, 75(4), 1068–1072, doi:10.1063/1.1666981.
- Tremsin, A., et al. (2005), Efficiency optimization of microchannel plate (MCP) neutron imaging detectors. I. Square channels with 10B doping, *Nucl. Instr. Methods Phys. Res. Sect. A*, 539(1–2), 278–311, doi:10.1016/j.nima.2004.09.028.
- Wetstein, J. (2012), Systems-level characterization of microchannel plate detector assemblies, using a pulsed, sub-picosecond laser, *Phys. Procedia*, 37, 748–756, doi:10.1016/j.phpro.2012.03.717.
- Wiza, J. L. (1979), Microchannel plate detectors, *Nucl. Instr. Methods*, 162, 587–601, doi:10.1016/0029-554X(79)90734-1.